AIAA 2002-0634

Laser Plasma Production and Expansion In A Supersonic Flow

K. Mori, K. Komurasaki, and Y. Arakawa
University of Tokyo
Tokyo, Japan

40th Aerospace Sciences Meeting & Exhibit

14-17 January 2002

Reno, Nevada

AIAA-2002-0634

Laser Plasma Production and Expansion in a Supersonic Flow

Koichi Mori[1], Kimiya Komurasaki[2], and Yoshihiro Arakawa[3]
University of Tokyo, Hongo 7-3-1 Bunkyo 113-8656, Japan

Abstract

Laser plasma was produced in a M=2 flow, in a quiescent standard atmosphere, and in a quiescent air at reduced pressure. The efficiency in producing an explosion was estimated from the shadowgraph images. In the M=2 flow, the efficiency was found 0.4. This value was almost same with that in the quiescent standard atmosphere. However, it decreased in the air at reduced pressure below 0.08MPa.

Electron density was measured by means of optical emission spectroscopy. It was found that the electron density increased with the ambient pressure, but was not influenced by the flow.

Introduction

Laser propulsion is expected as an alternative system for the launch at small cost. The air-breathing flight will be most fascinating, since a vehicle has not to load the propellants. Various kinds of laser propulsion system have been proposed. Pirri proposed and tested a thruster with a parabolic shell of revolution.[1] Similar thruster is now investigated by Shall, et al.[2] Another candidate "Light Craft" by Myrabo, et al. has a configuration similar to that of Air-breathing Pulse Detonation Engines,[3,4] and "LITA" is a laser-driven Ram-accelerator proposed by Sasoh, et al.[5]

In our previous report,[6] a conceptual "Far-field thruster" was studied, and its basic characters were investigated by experiments and one-dimensional computations. In the Far-field thruster, a high-power laser pulse is focused at the center of a hemispherical shell of revolution. Consequently, a breakdown occurs and plasma is produced at the focus. The exploding plasma drives a blast wave, which provides an impulsive thrust on the shell. On the other hand, a high-temperature "fireball" remains near the focus for a long period. By designing the shell to be larger than the diameter of the fireball, the thermal load on the shell can be suppressed. This feature of low-thermal load is the most fascinating aspect of the Far-field thruster.

The atmospheric air is loaded from the rear-side at a low-altitude and low-speed flight, and it will be loaded from the front-side at high-altitude and high-speed flight. The configuration of front-loading illustrated in Fig.1 can be called a Laser Ramjet. The pulsed-laser beam heats the atmosphere taken through the inlet, and the explosion occurs while the explosion center is blown downstream.

The design rules and the performance estimation for such components as inlet, plasma production chamber, and nozzle are now investigated by means of experiments and CFD simulations. For our final goal, four aspects should be clarified: (a) Efficiency of the inlet, (b) Efficiency in producing the explosion, (c) Nozzle efficiency, and (d) Over-all efficiency of the engine cycle. This paper will discuss especially on (b).

In the experiments on the rear-side loading thrusters,[1-5,7] the momentum coupling coefficient (the ratio of impulsive thrust to the laser pulse energy) has been measured using a thruster in simple geometries; plane-wall, and conical or parabolic nozzle of revolution. Pirri[1] introduced the energy conversion efficiency η_{ec}, which is the fraction of the input laser energy that is

[1] Graduate Student, Department of Advanced Energy, Student member of AIAA (e-mail: mori@al.t.u-tokyo.ac.jp)
[2] Associate Professor, Department of Advanced Energy, AIAA member
[3] Professor, Department of Aeronautics and Astronautics, AIAA member

converted into the kinetic energy of the exhausted gas. The momentum coupling coefficient depends both on η_{ec} and the exhausted mass. Pirri estimated these two variables respectively for the thruster of parabolic shell. However, the mechanisms of energy loss that determines η_{ec} have not been clarified yet.

In addition, the influence of real flight conditions on the laser-plasma production processes should be investigated: The plasma will be produced in supersonic flows at reduced pressure.

In this study, plasma was produced in a M=2 flow, in the quiescent standard atmosphere, and in a quiescent air at reduced pressure by focusing a CO_2 laser beam. The fraction of laser pulse energy that is converted into the blast wave energy was estimated, and electron density was measured to support the explanation for the dependency of the fraction on the ambient condition.

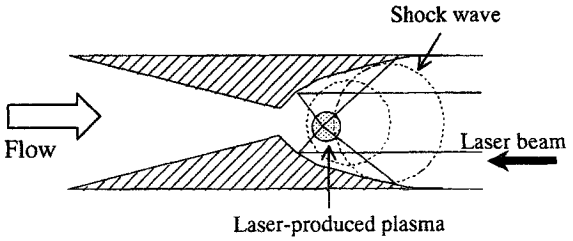

Fig.1. Schematic of Laser Ramjet

Model description

Some fraction of irradiated laser pulse energy E_i is transmitted through and/or reflected by the plasma, and the other fraction is absorbed in the plasma. The absorbed energy is converted into the expansion work acting on the ambient air, radiative loss, and frozen loss. The expansion work is converted into the kinetic and internal energy in the blast wave, which is equivalent to the explosion source energy, E_s. Efficiency in producing an explosion, η_s can be expressed as the fraction of E_i that is converted into E_s as,

$$\eta_s \equiv E_s / E_i \qquad (1)$$

Spherical blast wave has a self-similar structure, and its propagation is formulated by the theory of point blast explosion.[8] The time-varying radius of shock wave, $r(t)$ is expressed as,

$$r(t) = \xi_0 (E_s/\rho_0)^{1/5} t^{2/5} \qquad (2)$$

Here, ξ_0 is a constant value depending only on the gas composition, and it is 1.03 for the atmospheric air. ρ_0 is the ambient density. t is the time after the instantaneous energy input. The theory of point source explosion is valid as far as the shock strength is larger than a threshold p_{scr}/p_0 as,

$$p_s/p_0 > p_{scr}/p_0 \equiv \frac{\gamma+1}{\gamma-1} \qquad (3)$$

p_s is the pressure of the shock wave, and p_0 is the ambient pressure. γ is the specific heat ratio (1.4 for the atmospheric air.) The corresponding critical Mach number M_{cr} is 2.27 for air. The critical radius r_{cr} at which the shock wave reaches the critical Mach number corresponds to the boundary between the near-field and the far-field. r_{cr} is a function of the explosion source energy E_s and p_0, and from Eq.(2), it is written as,

$$r_{cr} = \left[\frac{2}{5^{2/3}} \xi_0^{5/3} \left\{ \frac{\gamma-1}{(\gamma+1)^2} \right\}^{1/3} \right] \left(\frac{E_s}{p_0} \right)^{1/3} \qquad (4)$$

From Eq.(4), E_s for air is calculated as,

$$E_s = 38.8 p_0 r_{cr}^3 \qquad (5)$$
$$= 8.1 p_0 V_{cr}$$

Since E_s is proportional to the critical volume of the shock compressed air V_{cr}, even when the shock wave propagates elliptically, an equivalent radius r_{eq} is useful to estimate E_s. It corresponds to the radius of the sphere, whose volume is same with that of the elliptic shock wave.

In addition, when t is defined as the period after the laser irradiation begins, the characteristic period for the energy input t_0 should be inserted into Eq.(2) as,

$$r(t) = \xi_0 (E_s/\rho_0)^{1/5} (t - t_0)^{2/5} \qquad (6)$$

E_s was estimated by fitting Eq.(6) to the t-r_{eq} profile.

Experimental apparatus and procedures

Laser and focusing optics

A TEA CO_2 pulsed-laser was used in the experiments. The laser pulse energy E_i was 10J/pulse, and was measured using a joule-meter before and after the experiments. Then, the shot-to-shot fluctuation of the laser pulse energy was maintained below 5% through the experiments. The laser pulse shape measured using a photon-drag detector (Hamamatsu photonics B749) is shown in Fig.2. A leading-edge spike appears, and an exponentially decaying tail follows. The shape is typical for TEA CO_2 pulse lasers. The full width at half maximum of the spike was 0.12 ± 20 μs, and the decay-constant of the tail was 1.15 ± 0.05 μs. The laser beam is in the high-order multi-transverse mode, and its cross section is a square of 30mm. The equivalent beam diameter was 34mm, which was the diameter of the circular beam having the same cross sectional area as the square beam.

The laser beam was focused in the air using an off-axial parabola mirror, whose focal length was 38.1mm, and the corresponding focusing F-number (≡ focal length/beam diameter) was 2.2. The mirror reflects an incident laser beam by 90 degrees along the optical axis into the focus.

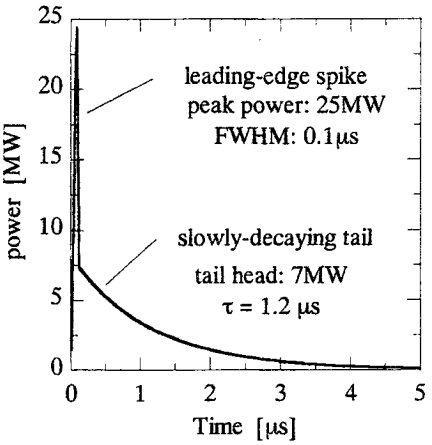

Fig.2 Laser pulse shape, E_i=10J/pulse

Wind tunnel

Plasma was produced in a supersonic wind tunnel. The picture and schematic of the wind tunnel are shown in Fig.3. The wind tunnel operated at M=2. The conditions of the flow are summarized in Table 1.

Dry air was compressed in a reserver tank up to 0.9MPa, and then, it was blown off the atmosphere through a header, a nozzle, and a test section. Total pressure was monitored in the header during the operation. Irradiation of the laser beam was started when the total pressure decreases to 0.8MPa.

The cross section of test section is a square of 40mm. The laser beam was introduced from the topside of the test section through a Zn-Se window.

The plasma was produced also in the quiescent air. The ambient pressure was changed from 0.01 to 0.1MPa to investigate the influence of the ambient pressure on η_s. The pressure was reduced using a rotary pump, and was monitored using a pressure gauge, which was placed at the bottom surface of the test section.

Shadowgraph system

The propagation of shock wave was visualized by means of shadowgraph, and η_s was estimated in each condition. The shadowgraph system is illustrated in Fig.4. Pictures were taken using an ICCD camera (Oriel Instruments InstaSpec™V ICCD detector, Model 77193-5). The image intensifier of the camera was operated as a shutter, and an optical emission from a gap-switch of the laser discharge tube was utilized to trigger the shutter: The strong emission from the gap-switch prior to the laser oscillation is detected by a photo-sensor through an optical fiber. The photo-sensor signal is transmitted to a delay-circuit (Stanford Research Systems, Inc. Digital Delay/Pulse Generator Model

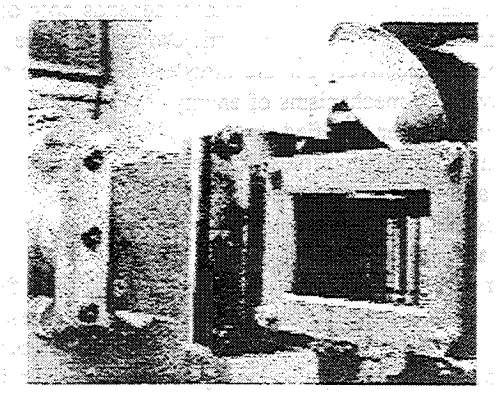

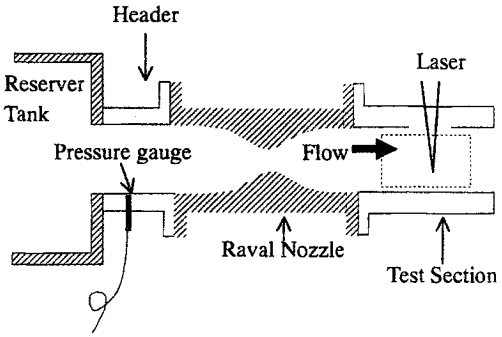

Fig.3 M=2 supersonic wind tunnel

Table 1 M=2 flow conditions

M_∞	2	
p_0 [MPa]	0.8	Total pressure
p_∞ [MPa]	0.1	$=1.0\times p_a$
ρ_∞ [kg/m^3]	2.3	$=1.8\times \rho_a$
T_∞ [K]	160	$=T_a/1.8$
U_∞ [m/s]	510	

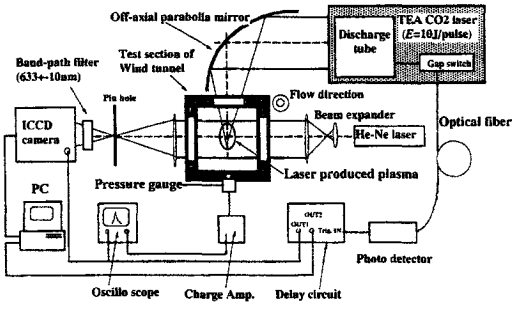

Fig.4 Schematic of shadowgraph system

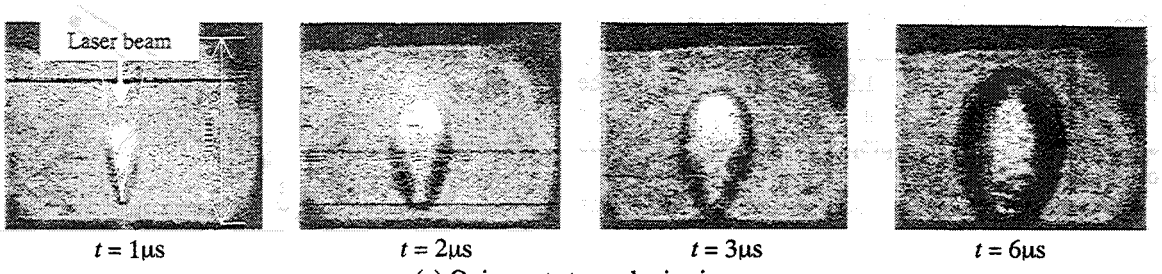

(a) Quiescent atmospheric air

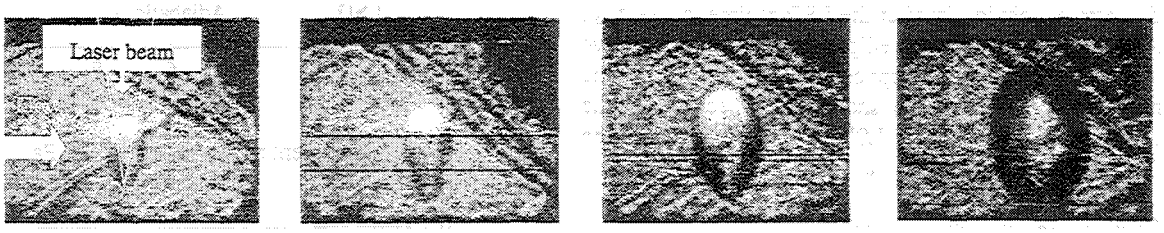

(b) M=2 flow

Fig. 5 Shadowgraph images

DG535), which enables us to take a picture with any delay period from the beginning of the laser pulse.

A He-Ne laser was used as a light source for the shadowgraphs. The emission from plasma has been decreased selectively by a band-path filter transmitting the wavelength of 633 ± 10 nm. However, the observed images were the superposition of the shadow of density gradient and the luminescence of plasma. Since the emission coefficient of bremsstrahlung radiation is proportional to the square of electron density, the emitting region in the images would be identical to the plasma one.

Measurement of Electron density

The electron density in the plasma region during the laser irradiance was estimated from the broadening of NI line. Although both the Doppler effect and the Stark effect can be dominant, the Stark broadening $\Delta\lambda_{1/2}$ and the shift $\Delta\lambda_s$ are formulated as,[9]

$$\Delta\lambda_{1/2} \approx 2\left[1+1.75\times10^{-4}N_e^{1/4}\alpha\left(1-0.068N_e^{1/6}T^{-1/2}\right)\right]10^{-16}wN_e \quad (10)$$

$$\Delta\lambda_s \approx \left[(d/w)+2.0\times10^{-4}N_e^{1/4}\alpha\left(1-0.068N_e^{1/6}T^{-1/2}\right)\right]10^{-16}wN_e \quad (11)$$

N_e and T are electron density and temperature, respectively. The Electron-impact half width w, relative electron-impact shifts d/w, and ion-broadening parameters α are tabulated by Griem as functions of the temperature.[10]

Three NI spectral lines of 742, 744, and 746 nm wavelength were used, and the electron density was deduced from the fitted Voigt functions using Eqs.(10) and (11). Since the dependency of the Stark broadening on the temperature is small, the temperature was assumed 1 eV.

The emission was introduced to a spectrometer PMA-50 (Hamamatsu photonics, Inc.) through an optical fiber. The spectrometer has a focal length of 50cm, and a grating of 1200 grooves/mm. The head of the optical fiber was placed at the side of the test section, and was aligned to detect all the emission from the plasma. The width of the slit placed in front of the grating, was set 20μm, and the exposure period was 0.4μs. The synchronization system was same with that for the shadowgraphs system noted above.

Results and Discussions

Shadowgraph images

The shadowgraph images in the quiescent standard atmosphere are shown in Fig.5 (a). Laser beam was focused from the top in each picture. After breakdown occurred in the vicinity of the focus, the Laser Supported Detonation (LSD) wave [11] traveled along the laser light channel in the direction opposite to the beam incidence at $t < 3\mu s$. The expansion of the shock wave was observed also in the direction lateral to the laser beam in this regime. As the laser power decayed, the LSD regime was altered to the Laser Supported Combustion (LSC) regime. At $t \geq 3\mu s$, the shock wave left the luminous plasma behind, and propagated farther. While the plasma front became to stay, its luminosity was decreased due to the decay in electron density.

The images shown in Fig.5 (b) were taken in the

M=2 flow. Breakdown and LSD/LSC transition occurred in the flow as well as in the quiescent condition. The shock wave traveled slightly slower than those in the quiescent condition. This is because the ambient density in the M=2 flow was 1.8 times larger than the atmospheric one as noted in Table 1. The propagation speed of the LSD wave is proportional to the -1/3 powers of the ambient density.

Since the propagation speed of the LSD wave was the order of 10,000m/s, and the flow speed was 510m/s, the effect of the flow itself was not expected significant in the LSD regime. However, the shock wave was blown downstream obviously after the LSD regime, at $t \geq 3\mu s$. As a result, the axis of the elliptically shaped shock wave inclined in the direction opposite to the flow. Since the propagation speed of the shock wave decayed to the order of 1000m/s after the LSD regime, the effect of the flow was expected to become significant at the stage.

Efficiency in producing an explosion

Estimated r_{eq} is plotted in Fig. 6 for both quiescent air and M=2 flow. r_{eq} in M=2 flow was slightly smaller than that in the quiescent condition. The solid curves in Fig.6 are deduced by fitting Eq.(6) at $3 < t < 10\mu s$. Since t_0 was found about 2μs, the heat addition occurred mostly at $t \leq 2\mu s$ during the LSD regime, and the shock expansion at $3 < t < 10\mu s$ can be considered adiabatic. As a result, E_s was found 4.0J in the quiescent condition, and 3.9J, in the M=2 flow.

From t-r_{eq} plots, η_s was estimated. The relation between η_s and the ambient pressure is shown in Fig.7. Open circles represent η_s in the quiescent conditions, and closed circles, in the M=2 flow. The dispersion on η_s was estimated less than 0.1. In the quiescent air, η_s increased from 0.2 to 0.5 with the ambient pressure p_0 until 0.08 MPa, and then began to decrease.

In the M=2 flow, η_s was 0.4, which was very close to the value in the quiescent standard atmosphere (p_0=0.1MPa).

Electron density

The line profile of NI emission is shown in Fig.8. Three lines were fitted with Voigt functions, and the electron density in the quiescent condition was estimated. The Stark broadening was larger than the wavelength resolution of the spectrometer at $N_e > 10^{22} m^{-3}$.

Electron density of the plasma produced in the quiescent air is plotted in Fig.9. At p_0=0.06 and 0.02MPa, N_e decayed during the LSD regime, and N_e at p_0=0.06MPa was always higher than that at p_0=0.02MPa.

This result suggests that the tendency of η_s at p_0<0.08MPa would be due to increase in N_e and decrease in the transmission loss with p_0.

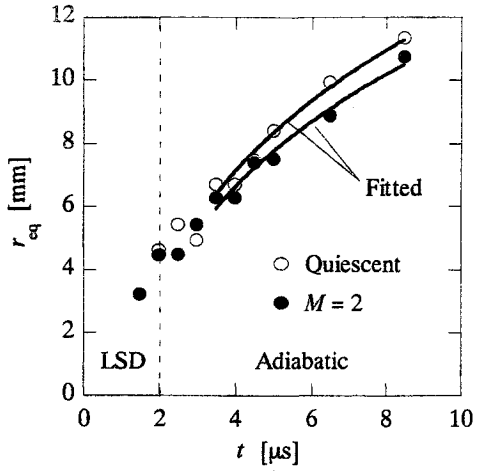

Fig.6 Equivalent radius r_{eq}, p_0 = 0.1MPa

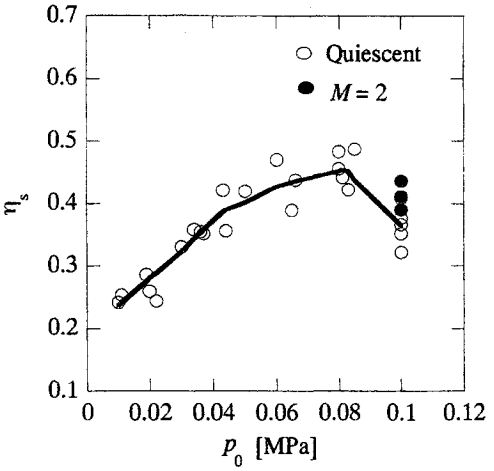

Fig.7 The relation between the ambient pressure and η_s

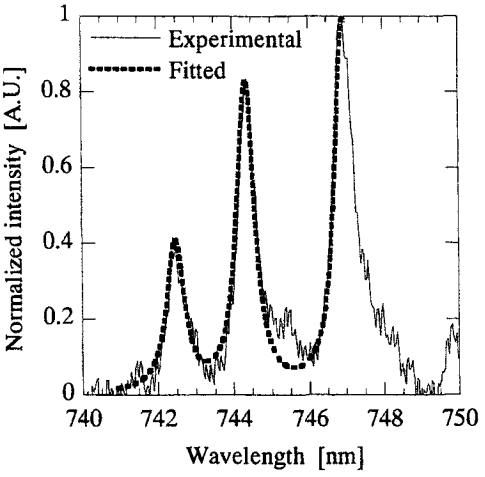

Fig.8 The line profile of NI emission, p_0=0.1MPa, t=4μs

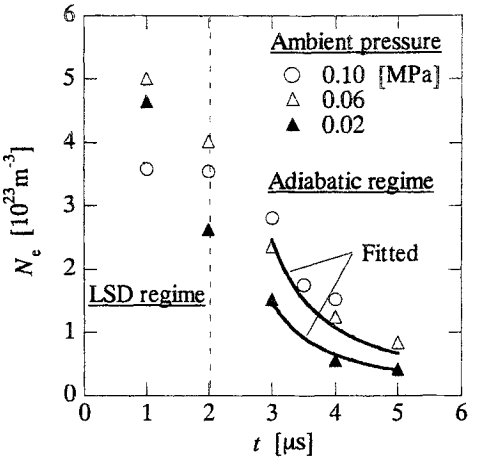

Fig. 9 Electron density in the quiescent air

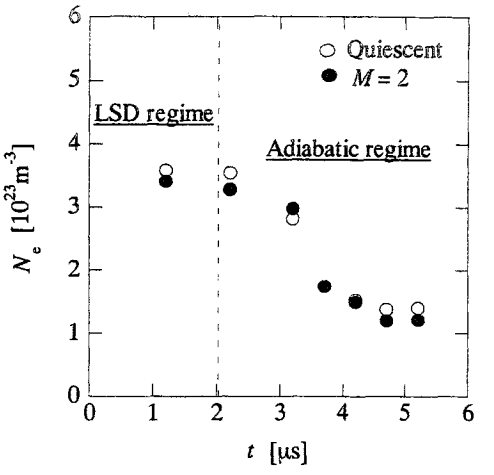

Fig. 10 Electron density in the M=2 flow and the quiescent standard atmosphere

In addition, N_e at p_0=0.1MPa kept a constant level during the LSD regime, and was lower than that at p_0=0.06MPa. The tendency of η_s at p_0>0.08MPa would be due to decrease in N_e with p_0.

Since the volume of the shock compressed air is proportional to $(t\text{-}t_0)^{6/5}$ in the adiabatic regime, the volume of plasma would also be proportional to $(t\text{-}t_0)^{6/5}$, and its density would decay proportionally to $(t\text{-}t_0)^{-6/5}$. The solid curves in Fig.9 were fitted with the equation,

$$N_e \propto (t - t_0)^{-6/5} \quad (12)$$

on the measured plots. Since the measured plots and the curves are very close to each other, the decay in N_e during the adiabatic regime would be controlled by the volumetric expansion.

N_e for the M=2 flow and the quiescent standard atmosphere is plotted in Fig.10. Since N_e for both conditions were very close to each other, the fractional absorption would not have been influenced by the flow.

In addition, it was found that the cutoff did not occur since the critical electron density for the cutoff is the order of 10^{25} m^{-3} for the CO_2 laser beam, whose wavelength is 10.6μm.

Summary

Both the fraction of the laser pulse energy that is converted into the blast wave energy, and the electron density in the M=2 flow were very close to those in the quiescent standard atmosphere.

On the other hand, in the quiescent air at reduced pressure, the fraction had a maximum at the ambient pressure of 0.08MPa. The electron density during the LSD regime also had same dependency on the ambient pressure with that of the fraction.

References

[1] Pirri, A.N., Monsler., M.J., and P.E. Nebolsine, "Propulsion by Absorption of Laser Radiation," *AIAA Journal*, Vol.12, No.9, Sept.1974, pp.1254-1261.

[2] Schall, W.O., Bohn, W.L., Eckel,H.-A., Mayerhofer, W., Riede, W., Zeyfang, E., "Lightcraft Experiments in Germany," proceeding of High-Power Laser Ablation III, Santa Fe, NM, USA, 2000.

[3] Myrabo, L.M., Messitt, D.G., and Mead, F.B., "Ground and Flight Tests of a Laser Propelled Vehicle," AIAA Paper 98-1001 (1998).

[4] Mead, F.B., and C.W. Larson, "Laser-Powered, Vertical Flight Experiments at the High Energy Laser System Test Facility," AIAA Paper 2001-3661 (2001).

[5] Sasoh, A., Kister, M., Urabe,N., and Takayama, K.,"LITA(Laser-driven In-tube Accelerator) Operation Under Elevated Pressure," AIAA Paper 2001-3666 (2001).

[6] Mori, K., Komurasaki, K., Katsurayama, H., and Arakawa, Y., "A Far-Field Repetitive Pulse Laser Thruster," AIAA Paper 2001-0649 (2001).

[7] Ageev, V.P., Barchukov, A.I., Bunkin,F.V., Konov, V.I.,Korobeinikov,V.P., Putjatin, B.V., and Hudjakov, V.M., "Experimental and Theoretical Modeling of Laser Propulsion," *Acta Astronautica*, Vol.7, 1980, pp79-90.

[8] Zel'dovich, Ya.B. and Raizer, Yu.P., *Physics of Shock waves and High-temperature Hydrodynamics Phenomena*, Academic Press, New York, 1967.

[9] LochteHoltgreven, W., *Plasma diagnostics*, AIP press, New York, 1995.

[10] Griem, H.R., *Plasma Spectroscopy*, McGraw-Hill, New York, 1964.

[11] Raizer, Yu.P., *Laser-Induced Discharge Phenomena*, Consultant Bureau Co. Inc., California, 1985.